ESOMAT 2009, 02032 (2009)
DOI:10.1051/esomat/200902032

3D strain fields surrounding Ni_4Ti_3: direct measurement and correlation with the R-phase.

W. Tirry[a1] and D. Schryvers[1]

COBO, KMS, Renaissancelaan 30, B-1000, Brussels, Belgium
[1] EMAT, University of Antwerp, Groenenborgerlaan 171, B-2020, Antwerp, Belgium

Abstract. Strain fields introduced by coherent Ni_4Ti_3 precipitates in austenitic Ni-Ti are believed to be a possible origin of why the R-phase transformation is introduced as an extra step before transforming to the B19'. The presence of this strain field was already confirmed in the past by conventional transmission electron microscopy (TEM) techniques and measured quantitatively by high resolution TEM (HRTEM). This time the geometrical phase method is applied on HRTEM micrographs to measure the full 3D strain tensor of the strain fields. Since each atomic resolution micrograph only results in a 2D measurement of the strain, observations in two different zone orientations are combined to retrieve the 3 x 3 strain tensor. In this work observations in a $[1\text{-}1\ 1]_{B2}$ and $[1\ 0\text{-}1]_{B2}$ zone orientation are used and this in case of precipitates with a diameter of around 50nm. In a next step the measured strain tensor is compared to the calculated eigenstrain of the R-phase in reference to the B2 matrix. This comparison shows that the introduced strain is very similar to the eigenstrain of one R-phase variant. Since for both structures, Ni_4Ti_3 and R-phase, four orientation variants are possible, each variant of the R-phase is thus able to accommodate the strain field of one of the Ni_4Ti_3 variants.

1. Introduction

The martensitic transformation of a Ni-Ti alloy, which is rich in Ni, e.g. 51at%Ni is strongly influenced by the thermomechanical history of the material. Whereas the basic transformation is the one transforming the cubic austenite phase to the monoclinic martensite one, also referred to as B2 and B19', respectively, it is possible to have multiple steps in the transformation [1-6]. A first step would be transformation to the so-called R-phase, which can be described as a rhombohedral distortion of the cubic matrix with a small shuffle of atoms. Extended studies have shown that when the Ni-rich material is aged around 500°C lens shaped Ni_4Ti_3 precipitates are occurring in the B2 matrix, their number and size dependant on the duration of the heat treatment [1,7,8]. After these heat treatments often (also depending on the duration) two transformation steps are occurring in the Differential Scanning Calorimetric (DSC) curves. In situ cooling experiments using synchrotron and neutron diffraction can relate this second peak to the R-phase transformation [9]. By using in-situ TEM cooling experiments it is seen that the R-phase nucleates first at the Ni_4Ti_3 precipitates present in the material [2,5,10,11]. TEM observations of the Ni_4Ti_3 precipitates reveal the presence of a strain field in the surrounding matrix in case of (semi)-coherent precipitates [2,12]. It is suspected that the strain fields introduced by these precipitates are beneficial for the transformation to the R-phase. Up to now the deformation of the area surrounding Ni_4Ti_3 precipitates was not measured or determined accurately enough to compare it directly with the deformation which would be introduced by the R-phase. In a previous work [12] a quantitative measurement of the strain field was made using atomic resolution TEM observations. The technique used was based on measuring differences in interplanar spacings from atomic resolution TEM micrographs using FFT based image processing. In this previous work the major intention was to measure magnitude and profile of the induced strains in order to compare it with the theoretical Eshelby model for elliptical inclusions. In the present work the focus is on the comparison of the induced elastic deformations by the precipitate with the transformation strain introduced when transforming to the R-phase. In order to do so Geometrical Phase Analysis (GPA) [13-15] was applied to HRTEM micrographs. The GPA method allows to retrieving the 2x2 deformation matrix from an atomic resolution image. By combining observations from two different crystallographic zone orientations the 3x3 deformation matrix can be reconstructed.

[a] e-mail: wim.tirry@ua.ac.be

Article available at http://www.esomat.org or http://dx.doi.org/10.1051/esomat/200902032

2. Experimental set-up

2.1 Specimen preparation

The as-received material has a composition equal to 51at% Ni and 49at% Ti and comes in the shape of a rod with a diameter of 3mm of which discs are cut with a thickness of 300µm. These discs are subjected to a heat treatment of 1h at 950°C in vacuum and water quenched, followed by an aging step in vacuum for 4h at 450°C and again water quenching. Subsequently, the discs are mechanically ground and prepared for TEM observations by electrochemical polishing using the double jet technique (Struers tenupol 3). The electrolyte is a mixture of 93% acetic acid and 7% perchloric acid at a temperature of 6°C for which a potential of appr. 20V is applied.

2.2 Transmission electron microscopy

High resolution images are obtained, using a top-entry JEOL 4000EX transmission electron microscope operated at 400kV and equipped with a LaB_6 filament. Micrographs are recorded on standard photographic plates in order to capture as much information as possible in a single exposure/image. Afterwards the negative or a selection of it is digitized by photographing it, using a digital reflex camera, directly from the negative or after a 3x optical enlargement. Using a negative scanner is another possibility, but was avoided in this case since the introduced modulation was more tedious to compensate for.

Since each HRTEM image of a specific zone axis only yields 2 of the 3 displacement vectors resulting in 3 of the 6 independent components of the symmetric strain matrix, observations along different crystallographic directions are necessary to result in 6 independent components. However, proper HRTEM imaging is in most cases only restricted to a few specific crystallographic zones allowing to resolving the two-dimensional projection of the lattice. Moreover, due to instrumental limitations it is in most cases not possible to tilt from one useful zone axis to another in the same area. Also, since we are interested in the strain distribution surrounding a precipitate the possible overlapping region at the interface between precipitate and matrix needs to be considered. Ideally, the zone axes that are chosen are those which have the habit plane interface edge-on, so that there is no area of overlap from which it would not be possible to measure any strains. In any case, one should take at least an orientation in which the inclination of the interface is minimal in order to keep this area of overlap as small as possible.

Considering all these aspects two families of zone axes are chosen: $\langle 101 \rangle_{B2}$ and $\langle 111 \rangle_{B2}$. From this point on only one variant is considered, being the one with following orientation relationship: $[100]_R$ // $[20\text{-}1]_{B2}$ and $(111)_R$ // $(111)_{B2}$, the subscripts R referring to the rhombic unit cell of the precipitate. This fixes the indices of the selected observation directions to: $[10\text{-}1]_{B2}$ and $[1\text{-}11]_{B2}$. The $[10\text{-}1]_{B2}$ zone images the habit plane edge-on and in case of the $[1\text{-}11]_{B2}$ zone the habit plane is inclined with an angle of 19.37° as illustrated in Figure 1.b. This combination of zone axes is chosen since they are perpendicular to each other. Nevertheless, due to crystal symmetry and the matrix-precipitate orientation relationship observations made in the $[1\text{-}11]_{B2}$ and $[10\text{-}1]_{B2}$ orientation can also be regarded as made in a $[\text{-}111]_{B2}$, $[11\text{-}1]_{B2}$ respectively $[1\text{-}10]_{B2}$, $[01\text{-}1]_{B2}$ orientation. Moreover, in this work only coherent and semi-coherent precipitates are considered, which means they have a diameter smaller than around 300µm [16].

2.3 Strain measurement

An elaborated description of the GPA technique can be found in [13-15], but since it is a relatively new method, the basic concept is explained briefly. By using a sequence of Fast Fourier Transforms (FFT) of the digitized images, applying masking windows and inverse FFT transformations the geometric phase of a chosen lattice reflection g can be retrieved in each pixel of the image. It is proven that this geometric phase is equivalent with the displacement in the chosen g direction and this in relation to a user defined reference area in the same image. By performing this operation for two different g's the displacement vector can be retrieved in each pixel of the image, allowing to calculate the two-dimensional deformation matrix, including rotations. By decomposing this in its symmetric and anti-symmetric part strain components ε_{xx}, ε_{yy}, ε_{xy} can be determined in each pixel. The spatial resolution is of course not equal to the pixel size, but determined by the masking windows used to select the g-reflection. A Gaussian selection window is applied in the present case and the algorithm used to estimate the spatial resolution is found in [15] and is mainly determined by the diameter of the window. On the one hand a larger window radius would enhance the spatial resolution, but on the other hand more noise is included resulting in a worse precision on the strain components. As such a trade off should be made and in our case a window resulting in a spatial resolution of 3nm allowed an acceptable signal to noise ratio. One should take into account that the projector lens of a TEM [17] and the digitization of the negative are introducing extra deformations in the image, which should be compensated for. In order to do so a Ni-Ti reference sample was used in which no deformations are expected. Atomic resolution images of this sample are recorded with a same

microscope alignment and digitized in the same way as the other images. As a consequence the deformations measured in this image are due to the recording and subsequent digitization procedure and are a standard to correct the other images. These deformations are a function of position (smooth and continuous) and are increasing towards the edges of the negatives; strains up to 2% and rotations up to 1.5° are introduced depending on the microscope used. Since the expected deformations are of this magnitude it is indispensable to correct for these phantom strains. First define D(x,y) to be the deformation matrix introduced by mainly the projector lens and subsequent digitization procedures, E(x,y) the deformation measured from the digitized image and Er(x,y) the real deformation present in the material. This real deformation Er(x,y) is then obtained by applying the algorithm $Er(x,y) = D^{-1}(x,y)E(x,y)$ for all pixels x,y. The D(x,y) matrices are obtained from an experimental image and as such are rather noisy and not smooth. Since the distortions introduced are expected to be smooth and continuous a smoothing is applied to the D(x,y) data before applying them on the actual image [17].

3.Results

3.1 Strain measurements

Figure 1.a shows the image of two small precipitates of a same variant type and with a diameter of around 50nm. The area indicated by the square is the reference area, known to correspond with undeformed matrix using the technique presented in previous work [12]. As such all deformations measured are in reference to the relaxed B2 structure. The x,y,z reference frame is chosen in such a way that the x-direction corresponds with the $[121]_{B2}$ direction being perpendicular to the trace of the interface plane, the y-direction corresponds to the $[10\text{-}1]_{B2}$ direction which is parallel to the interface plane. The z-axis is the direction of observation being the $[1\text{-}11]_{B2}$ zone orientation. Figure 1.c shows the strain map for the ε_{xx} component, showing that there are tensile strains close to the precipitate and compressive strains at the tip. In order to have an acceptable precision on the strain components they are averaged over a square area, which has a dimension at least larger than the spatial resolution (e.g., 3nm). In the present case 5nm was chosen. In case for the area indicated by the white square in Figure 1.c this results in: ε_{xx} = (0.0086 +- 0.0018), ε_{yy} = (-0.0046 +- 0.0016), ε_{xy} = (0.0003 +- 0.0015). It can be noticed from these values that when there is a tensile strain present in the x-direction there is a compression in the y-direction strongly indicating these strains have an elastic nature.

A similar observation was made in a $[1\ 0\text{-}1]_{B2}$ zone and is shown in Figure 1.b. In this case the reference frame is chosen as follows: x // $[111]_{B2}$ being perpendicular to the interface plane and y // $[1\ \text{-}2\ 1]_{B2}$.
A mapping of the ε_{xx} strain component is shown in Figure 1.d and shows a similar shape as in the case of the $[11\text{-}1]_{B2}$ zone observation. A measurement of the strain component in the area indicated by a white square of 5nm x 5nm results in: ε_{xx} = (0.0109 +- 0.0038), ε_{yy} = (-0.0042 +- 0.0018), ε_{xy} = (-0.0003 +- 0.0013). Again tensile strains are measured in the x-direction accompanied with a compressive strain in the y-direction, which is consistent with the other measurements and an indication of elastic strain.

3.2 Full strain matrix calculation

By combining the 2x2 strain matrices obtained from the two different zone observations the 3x3 strain matrix can be reconstructed. In practice this reconstruction is performed by the following scheme. First, a reference system is chosen in which the strain matrix E is represented, in this case; x // $[100]_{B2}$, y // $[010]_{B2}$, z // $[001]_{B2}$ being the reference frame of the cubic unit cell. Second, in order to determine the 6 independent components of E from the 6 measured values, a system of equations should be solved. These equations are obtained by transforming E to the reference systems in which the observations are made. Each of these reference systems provides three independent equations, expressing the measured values in the six strain components of the basic reference frame. As mentioned before, due to crystal-precipitate symmetry, observations in the $[10\text{-}1]_{B2}$ and $[1\text{-}11]_{B2}$ zone orientation can not be discriminated from those of the two other orientations. As such, more than 6 equations are available of which 6 independent ones are chosen to retrieve the full deformation matrix E in the chosen cubic reference frame.

The evaluation is performed for the area indicated by the white squares, for both are at the same distance of the precipitate and in case for the $[1\text{-}11]_{B2}$ zone it is far enough from the interface not to have overlap with the matrix. In addition, the measurements are taken close to the central axis of the precipitate. The values of the measured strains at this position are introduced in equation 1 and result in a strain matrix E shown below (the precision on these values is discussed further below).

$$E = \begin{pmatrix} 0.0017 & 0.0048 & 0.0051 \\ 0.0048 & 0.0012 & 0.0055 \\ 0.0051 & 0.0055 & -0.00073 \end{pmatrix}$$

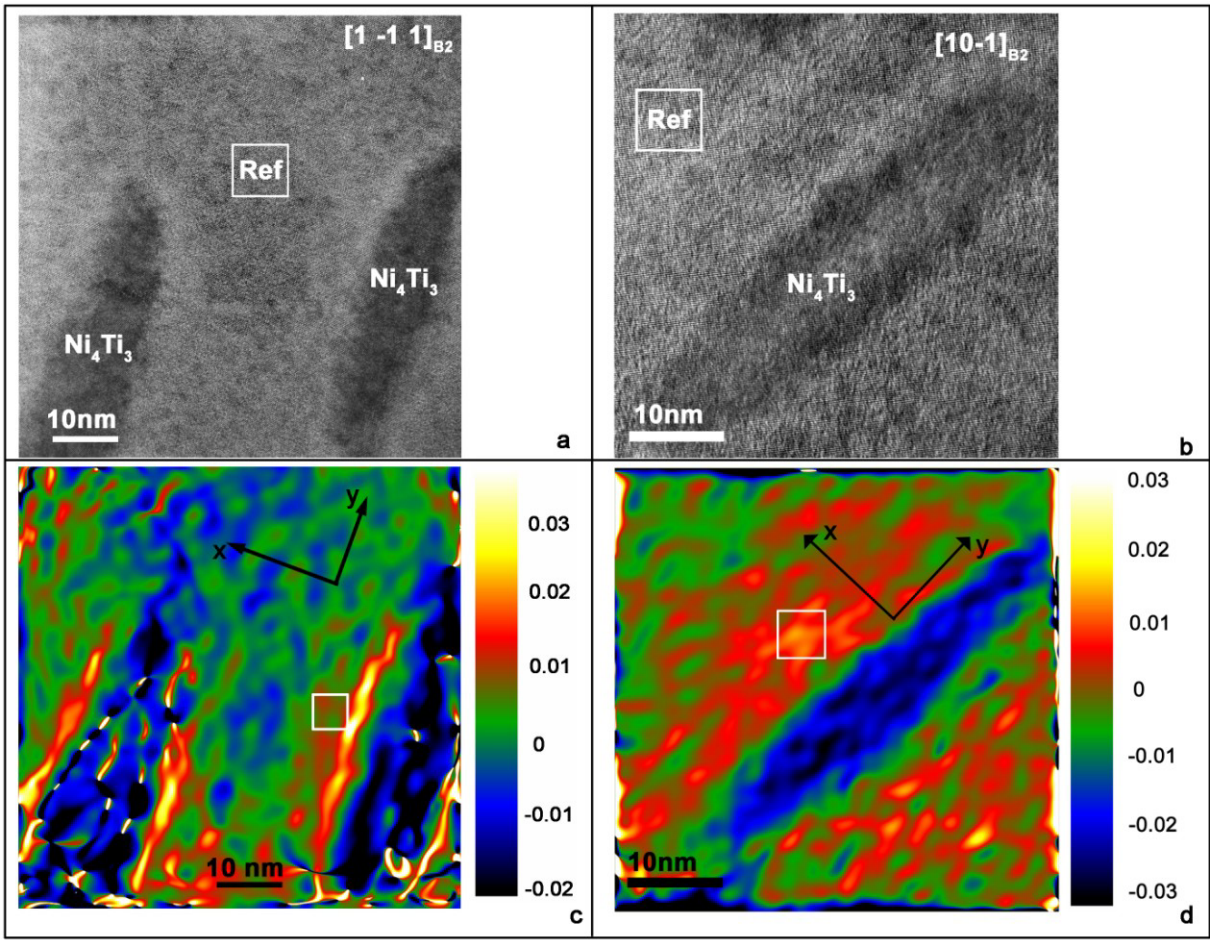

Fig. 1. (a,b) Atomic resolution images in a $[1\text{-}1\ 1]_{B2}$ and $[10\text{-}1]_{B2}$ zone orientation, (c,d) strain maps revealing the 2D deformations surrounding the precipitates.

4. Discussion and conclusions

The reconstructed 3x3 matrix E can now be compared with the eigenstrain of the R-phase in reference to the B2 matrix. A method on how this eigenstrain can be retrieved is described in [9,18]. In order to calculate this eigenstrain as accurate as possible, accurate lattice parameters for the B2 and R-phase are needed. In case of a nominal matrix composition of $Ni_{50.7}Ti_{49.3,}$ i.e. close to the material used in this work, these are: a_{B2} = 0.30141nm and a_R = 0.73388nm, c_R = 0.52838nm [9]. Since the R-phase has a lower symmetry than the cubic one, 4 orientation variants are possible which is similar to the case of the precipitate. These 4 variants are given in Table 1. The eigenstrain matrix of R-phase orientation variant 1 is very similar to the reconstructed one: in both cases the values on the diagonal are close to zero while the remaining values are positive and of the same order of magnitude (among one another as well as with respect to the calculated values) which indicates that we are dealing with the same strain states.

In this entire discussion it is important to consider the precision on the measured and reconstructed values in the 3D strain matrix. The latter are calculated using standard uncertainty propagation theory on the exact analytical solution of the system, which are linear equations of the measured strain values. In case of the measured values precision is defined as the standard deviation on the average strain value over a $(5x5)nm^2$ domain and has values between 0.0013 and 0.0038. However, due to propagation some of the reconstructed values get a far worse precision compared to the measured ones. In this case, the worst precision is obtained on the Exx component, being 0.0017±0.046, which is far larger than the strain value itself. The best precision in this case is obtained on the Exz component being 0.0051±0.0017 which is comparable to the one of the measurements. It was computed that in order to have a precision below 0.0017 on all the reconstructed E components, all measured strain values should have a precision of 0.0001, which can not be obtained with the GPA method.

R-phase variant 1	R-phase variant 2
$R1 = \begin{pmatrix} 0.0001 & 0.0060 & 0.0060 \\ 0.0060 & 0.0001 & 0.0060 \\ 0.0060 & 0.0060 & 0.0001 \end{pmatrix}$	$R2 = \begin{pmatrix} 0.0001 & -0.0060 & -0.0060 \\ -0.0060 & 0.0001 & -0.0060 \\ -0.0060 & -0.0060 & 0.0001 \end{pmatrix}$
R-phase variant 3	R-phase variant 4
$R3 = \begin{pmatrix} 0.0001 & 0.0060 & -0.0060 \\ 0.0060 & 0.0001 & -0.0060 \\ -0.0060 & -0.0060 & 0.0001 \end{pmatrix}$	$R4 = \begin{pmatrix} 0.0001 & -0.0060 & 0.0060 \\ -0.0060 & 0.0001 & -0.0060 \\ 0.0060 & -0.0060 & 0.0001 \end{pmatrix}$

Table 1. Representation of the eigenstrain matrices of the 4 R-phase orientation variants in the $[100]_{B2}$, $[010]_{B2}$ and $[001]_{B2}$ reference system.

Since there is such a strong correspondence between the elastic strain induced by the precipitate and the shape deformation corresponding with variant 1 of the R-phase transformation it is suggested that the R-phase might indeed properly accommodate the strain field induced by the precipitate.

Due to symmetry each of the four possible orientation variants of the R-phase will be able to accommodate the strain field introduced by one of the four orientation variants of the precipitate, confirming a hypotheses made in [9]. Transformation of the matrix to this variant is beneficial for the global energy of the system since the strain accompanied due to transformation to the R-phase will replace the elastic strained matrix. Of course the full energy balance should be made between the elastic energy, the transformation energy and the free energy difference between the B2 and R-phase to calculate the temperature at which this will take place.

In-situ cooling experiments indeed show that transformation to single and twinned variants of the R-phase takes place in close vicinity of the Ni_4Ti_3 precipitates [2,10,11]. However, no accurate data is available concerning which variants are present and which twin variants are occurring. The measurements here indicate that the induced strain could be compensated by one R-phase variant. Nevertheless, a twinned structure is most likely to occur since at the B2-R interface compatibility has to be maintained, and in case of a martensitic transformation twinning of the martensite (or in this case R-phase) is a classic mechanism to achieve this.

Changes in concentration or a possible gradient in the close vicinity of the precipitates are not considered in this work, but they might as well affect the transformation behavior of this material. These topics are discussed in related works [19,20].

The authors are well aware that an electron transparent area should be considered as a thin film and there could be a difference in strain field surrounding a precipitate located in a thin film compared to the original one in the bulk case. However, observations of the R-phase nucleating at the precipitates were also made in a TEM sample and as such the two observations are consistent with one another even if the strain field would be altered in the thin film case. Nevertheless, there will be a consequence on the reconstructed 3D strain matrix since the two different observation directions will exhibit a different relaxation behavior of the elastic field. More information on the possible influence of this relaxation is given elsewhere [21], however, the main conclusion remains that the elastic strain field remains similar to the eigenstrain of the R-phase.

Acknowledgements
This work was funded by the Inter University Attraction Poles program (Belgian Science Policy) under contract number P6-24.

References

[1] J. Khalil-Allafi, A. Dlouhy, G. Eggeler, Acta. Mat. **50** (2002)
[2] L. Bataillard, J.-E. Bidaux, R. Gotthardt, Phil. Mag. A **78(2)** (1998).
[3] M. C. Carroll, Ch. Somsen, G. Eggeler, Scripta Mat. **50** (2004)
[4] G. Fan, W. Chen, S. Yang, J. Zhu, X. Ren, K. Otsuka, Acta Mat. **52** (2004)
[5] J. Michutta, Ch. Somsen, A. Yawny, A. Dlouhy, G. Eggeler, Acta Mat. **54** (2006)
[6] H. Morawiec, J. Ilczuk, D. Stro´z˙, T. Goryczka, D. Chrobak, J. Phys. IV Fr **7(C5)** (1997)
[7] M. Nishida, C.M. Wayman, T. Honma, Met. Trans. A **17** (1986)
[8] T. Tadaki, Y. Nakata, K. Shimizu, and K. Otsuka, JIM **27(10)** (1986)
[9] J. Khalil-Allafi,W.W. Schmahl, M.Wagner, H. Sitepu, D. M. Toebbens, G. Eggeler, Mater. Sci. Eng. A **378** (2004)
[10] A. Dlouhy, J Khalil-Allafi, G Eggeler, Phil. Mag. A **3** (2003)
[11] D. Stróż, Proceedings of EMC 2004, 13the European Microscopy Congress, (2004)
[12] W. Tirry, D. Schryvers, Acta Mat. **53** (2005)
[13] M. J. Hÿtch, Scan. Micr. **11** (1997)
[14] M. J. Hÿtch, E. Snoeck, R. Kilaas, Ultramicr. **57** (1998)
[15] J.L. Rouvière, E. Sarigiannidou, Ultramicr. 106 (2005) 1.
[16]K. Gall, H. Sehitoglu, Y. I. Chumlyakov, J. V. Kireeva, H. J. Maier, J. Eng Mater. Technol. **121** (1999)
[17]] F. Hüe, C. L. Johnson, S. Latigue-Korinek, G. Wang, P. R. Buseck, M. J. Hÿtch, J. electr. Mic. **54** (2005)
[18] K. Bhattacharya, *Microstructure of Martensite, why it forms and how it gives rise to the shape-memory effect.* (Oxford Univ. Press, 2003)
[19] Z. Yang, W. Tirry, D. Lamoen, S. Kulkova, D. Schryvers, Acta. Mat. **56,** (2008).
[20] Z. Yang, W. Tirry, D. Schryvers, Scripta Mat. **52,** (2005)
[21] W. Tirry, D. Schryvers, Nature Mat. accepted for publication (2009)